대한설비공학회 2008 하계학술발표대회 논문집 pp. 1358 ~ 1365

08-R-004

Numerical Study of the Snubber of Reciprocating Hydrogen Compressing System

M. Sq. Rahman*†, Gyeonghwan Lee*, Hanshik Chung** and Hyomin Jeong**

*† *Department of Mechanical and Precision Engineering, Gyeongsang National University, Tongyeong 650-160, Korea*

** *Department of Mechanical and Precision Engineering, Gyeongsang Nationaal University, Institute of Marine Industry, Tongyeong 650-160, Korea*

ABSTRACT: By Computational Fluid Dynamics simulation, general information about an internal gas flow can be achieved. This will be very useful to improve flow inside the pipes and snubber system. Relating with hydrogen compressing system, which plays an important role in hydrogen energy utilization, this method should be a powerful tool to observe the flow quickly and clearly. Flow pressure characteristic analysis of hydrogen gas flowing through the snubber of a reciprocating compressor is presented in this paper. The CFD calculation of pressure pulsation and pressure loss are very close to the experiment. Therefore, consequently development of the better hydrogen compressing system will be observed with better understanding by CFD.

Key words: hydrogen compressing system, snubber, amplitude, RMS, CFD

NOMENCLATURE

t : time [s]
x_i : cartesian coordinate (i = 1,2,3)
u_i : absolute fluid velocity component in direction xi [m/s]
p : piezometric pressure = ps-ρ0 gmxm [Pa]
p_s : static pressure [Pa]
ρ_0 : reference density [kg/m3]
g_m : gravitional acceleration [m/s2]
x_m : coordinate relative to datum where ρ0 is defined
ρ : density [kg/m3]
τ_{ij} : stress tensor component [Pa]
s_m : mass source component [kg/m3s]
s_i : momentum source component [kg/m2s3]
δ_{ij} : kronecker delta, is unity when i = j and zero otherwise.

† Corresponding author
Tel.: +82-55-646-4766; fax: +82-55-640-3188
E-mail address: msqr69@yahoo.com

1. Introduction

Hydrogen produced through non-fossil fuel sources by using the different forms of sustainable energy sources, such as solar, hydropower, wind, nuclear, etc. (so-called green energy based hydrogen production), is considered to be a prime fuel in supply and security, transition to hydrogen economy, environmental betterment, and social, societal, technological, industrial, economical and governmental sustain abilities in a country. Thus, green energy based hydrogen system can be one of the best solutions for accelerating and ensuring global stability and sustainability. Therefore the production of hydrogen from non-fossil fuel sources and the development and application of green energy technologies become crucial in this century for better transition to hydrogen economy.[1]

The assertion of "hydrogen is considered a

promising future fuel for vehicles" is based on three main arguments: the potential reducing greenhouse gases from the transport sector, greater energy supply security, i.e. hydrogen can be produced from many energy sources and hence the risk of shortage of supply may be reduced; the potential of zero local emissions with the use of fuel cells.

The absence of hydrogen infrastructure is seen as major obstacle to the introduction of hydrogen FCVs. A full scale hydrogen infrastructure with production facilities, a distribution network and refueling stations is costly to build. The venture of constructing a hydrogen refueling infrastructure constitutes a long-term, capital-intensive investment with great market uncertainties for FCVs. Therefore, reducing the financial risk is major objective of any long-term goal to build a hydrogen infrastructure.[2]

All fuel cells currently being developed for near term use in road vehicles require hydrogen as a fuel. While hydrogen can be produced onboard the vehicle by reforming methanol or gasoline, direct storage of compressed gaseous hydrogen has many attractive features. They are simpler vehicle design, less costly and more energy efficient, refueling can be accomplished rapidly, and hydrogen can be produced from many sources.[3]

The relative simplicity of vehicle design for the hydrogen fuel cell vehicle must be weighed against the added complexity and cost of developing a hydrogen refueling and infrastructure. Unlike gasoline and natural gas, hydrogen is not widely distributed to consumers today, and refueling a large number of hydrogen vehicles poses significant challenges. The question is often asked, 'Where is the hydrogen going to come from?' Indeed, hydrogen infrastructure is sometimes perceived as a 'show-stopper' for hydrogen vehicles. One of the most important processes in the hydrogen gas handling is the compressing system. This process is needed in all step of hydrogen gas energy utilization: production, storage, distribution until using. In addition since hydrogen will replace the role of fossil fuel, so all approach done in this field should be rewarded. This paper presents the numerical study about gas flow characteristics in snubber system of reciprocating hydrogen gas compressor.

2. Methodology

2.1 Experimental Set up

A snubber was constructed by acrylic material. It had one inlet pipe, one outlet pipe and one tube shaped unit. There were made 3 pressure measuring points in inlet and outlet pipe at proper distance. An acryl flat plate of specified height, thickness and width was located inside the tube shaped unit at proper angle. The geometrical data of snubber is shown in Figure 1. Pressure measuring transducer was installed at each point for taken pressure values. The inlet pipe was connected to the compressor using a small hose pipe and its outlet was exposed to the atmosphere. The experimental setup for its different components was as in Figure 2. The experiment was conducted by running the compressor and setting motor frequency at 10, 20, 30, 40, 50, and 60 Hz. Pressure value was sensed by pressure sensor, amplified and recorded in a PC using data logger.

Hydrogen gas has same character with the atmospheric air. Especially to observe the pressure from physical approach (without considering the chemical character), pressured air can be used to represent hydrogen gas. Air and hydrogen gas have almost the same compressibility character. So, air compressor was used in this experiment.

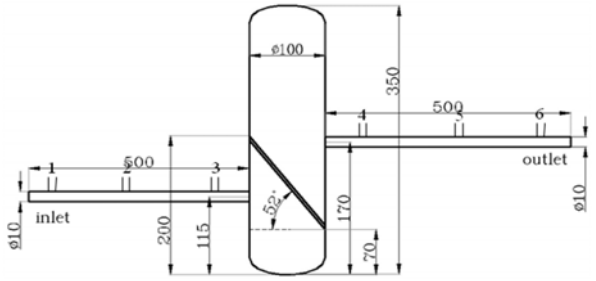

Fig. 1 Snubber dimensions with pressure measuring points

2.2 Method

Motor driven reciprocating pump was used in this experiment. The rotation of motor was controlled by its frequency regulator. The maximum motor rotation was 1800 rpm at maximum frequency (60 Hz). The compressor rotation and its frequency can be found as in eq. (1) and eq. (2).

$$\omega_{comp}[rpm] = f_{set}[Hz] \times 12.84[rpm/Hz] \quad (1)$$

$$f_{comp}[Hz] = f_{set}[Hz] \times 0.214 \quad (2)$$

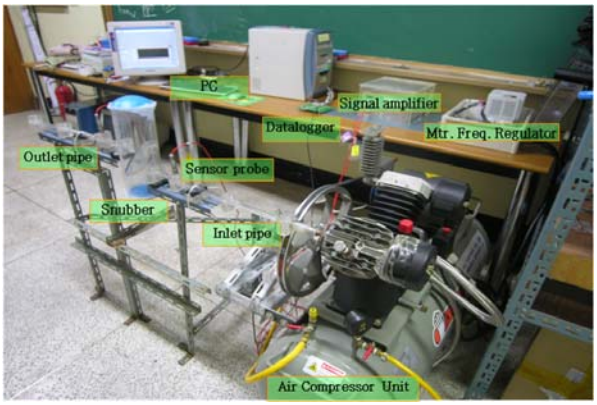

Fig. 2 Experimental set up

The periodic action of propelling gas through a pipe by the to and fro movement of the piston in the cylinder in reciprocating compressor caused pulsation. The piston-crank-valve mechanism generates a variable pressure, which over time creates a composite pressure wave in the suction and discharge pipe. This composite wave is made up of a number of waves. Due to periodic wave generation, multiple frequencies of pulsation are created that causes the force of vibration in the whole system.

Pressure produced by a piston in reciprocating compressor is fluctuating. The fluctuating of pressure and its amplitude can be calculated as eq. (3) and eq. (4).

$$p = \frac{p_{\max} + p_{\min}}{2} \quad (3)$$

$$A = \frac{p_{\max} - p_{\min}}{2} \quad (4)$$

Same with the other gas line utilities, gas that passing through a snubber will be reduced in pressure and reduced in pressure fluctuation. It is related to the amplitude of pressure. The pressure reduction or loss and amplitude reduction can be expressed in the percentage by the eq. (5) and eq. (6), respectively.

$$P_{red}(\%) = \frac{P_{in} - P_{out}}{P_{in}} \times 100\% \quad (5)$$

$$A_{red}(\%) = \frac{A_{in} - A_{out}}{A_{in}} \times 100\% \quad (6)$$

Experimental data at every section were collected using data logger and analyzed them. Data at point 3 and point 4 were analyzed for pressure loss and amplitude reduction. The RMS values of input and output of pressure were used for pressure loss. FFT analysis was done to on data to find out amplitude values of the pressure waves along the snubber. The resultant value of the variables was calculated by taking square root of summation of squares of all values.[4] The pressure and the pressure pulsation reduction were obtained by eq. (5) and eq. (6) using data from experiment.

2.3 Computational Methodology

A numerical solution is the final result of two steps: a modeling of the physical phenomena so as to obtain a set of PDEs (physical or mathematical model), and the conversion of these PDEs to algebraic equations on their solution on a computer (computational model). The first step concerns modeling research such as turbulence modeling and modeling of chemical kinetics. The second step involves the discritization of PDEs, the numerical procedures to solve the algebraic equations, the programming of the code, the criteria for finishing the convergence procedure and the computer accuracy. The errors introduced in the second are known as computational errors and the process to study these errors as verification process. Once the mathematical model and the computational model have been independently verified, the final validation of the simulation process should be carried out by comparing the results predicted by the simulation with experimental data, which is known as validation process. In this context, validation process is the last step of the overall procedure required to assess credibility. In validation process, uncertainties arise in both the experimental results and the computational results. Therefore, when analyzing discrepancies between simulation and experimental data, attention must be focused not only on the numerical solution (mathematical model and computational model), but also on the procedure adopted to obtain the experimental data. A simulation is developed on pertinent mathematical model. As an effort of quantifying physical phenomena, once it has been built. It is generally recognized that all existing turbulence models are inexact representations of the physical phenomena of turbulence. The degree of approximation in a given model depends on the nature of the flow to which it is being applied, and the characterization of the circumstances which give rise to 'good' and 'bad' performance must unfortunately be based mainly on experience.[5]

Eddy viscosity turbulence models are based on the analogy between the molecular gradient-diffusion process and turbulent motion (Boussinesq model). The Reynolds stresses and turbulent scalar fluxes in these models are directly linked to the local gradients of the mean flow field through a turbulent viscosity determined by a characteristic turbulence velocity scale and length scale are very numerous, ranging from prescribed profiles to the profiles to the popular two-equation models. Special models are also employed to characterize the flow near walls.

k-epsilon model comprising transport equations for the turbulence kinetic energy k and its dissipation rate ε. In these models, k and ε are chosen as typical turbulent velocity scale and length scale, respectively. The options differ from each other in one of the following respects:

- The form of the equations
- The treatment of the near-wall region
- The relation between Reynolds stresses and the rates of strain.

Those models that use a linear relationship between Reynolds stresses and strains are classified as non linear.

Conservation of mass

$$\frac{\partial \rho}{\partial t} + \frac{\partial}{\partial x_j}\left(\rho u_j\right) = s_m \tag{7}$$

Conservation of momentum (Navier-Stokes equation)

$$\frac{\partial \rho u_i}{\partial t} + \frac{\partial}{\partial x_j}\left(\rho u_j u_i - \tau_{ij}\right) = -\frac{\partial p}{\partial x_i} + s_i \tag{8}$$

$$\tau_{ij} = 2\mu s_{ij} - \frac{2}{3}\mu \frac{\partial u_k}{\partial x_k}\delta_{ij} - \overline{\rho u_i' u_j'} \tag{9}$$

$$s_{ij} = \frac{1}{2}\left(\frac{\partial u_i}{\partial x_j} + \frac{\partial u_j}{\partial x_i}\right) \tag{10}$$

Turbulence kinetic energy

$$\frac{\partial}{\partial t}(\rho k) + \frac{\partial}{\partial x_j}\left[\rho u_j k - \left(\mu + \frac{\mu_t}{\sigma_k}\right)\frac{\partial k}{\partial x_j}\right] =$$

$$\mu_t\left(P + P_B\right) - \rho\varepsilon - \frac{2}{3}\left(\mu_t \frac{\partial u_i}{\partial x_i} + \rho k\right)\frac{\partial u_i}{\partial x_i} + \mu_t P_{NL} \tag{11}$$

where

$$P \equiv S_{ij} \frac{\partial u_i}{\partial x_j} \tag{12}$$

$$P_B \equiv -\frac{g_i}{\sigma_{h,t}} \frac{1}{\rho} \frac{\partial \rho}{\partial x_i} \tag{13}$$

$$P_{NL} = -\frac{\rho}{\mu_t} \overline{u_i' u_j'} \frac{\partial u_i}{\partial x_j} - \left[P - \frac{2}{3} \left(\frac{\partial u_i}{\partial x_i} + \frac{\rho k}{\mu_t} \right) \frac{\partial u_i}{\partial x_i} \right] \tag{14}$$

P_{NL} = 0 for linear models and σ_k is the turbulent Prandtl number. The first term on the right-hand side of equation (11) represents turbulent generation by shear and normal stresses and buoyancy forces, the second viscous dissipation, and the third amplification or attenuation due to compressibility effects. The last term accounts for the non-linear contributions.

Turbulence dissipation rate

$$\frac{\partial}{\partial t}(\rho\varepsilon) + \frac{\partial}{\partial x_j}\left[\rho u_j \varepsilon - \left(\mu + \frac{\mu_t}{\sigma_\varepsilon} \right) \frac{\partial \varepsilon}{\partial x_j} \right] = C_{\varepsilon 1} \frac{\varepsilon}{k} \left[\mu_t P - \frac{2}{3} \left(\mu_t \frac{\partial u_i}{\partial x_i} + \rho k \right) \frac{\partial u_i}{\partial x_i} \right] + C_{\varepsilon 3} \frac{\varepsilon}{k} \mu_t P_B - C_{\varepsilon 2} \rho \frac{\varepsilon^2}{k} + C_{\varepsilon 4} \rho \varepsilon \frac{\partial u_i}{\partial x_i} + C_{\varepsilon 1} \frac{\varepsilon}{k} \mu_t P_{NL} \tag{15}$$

Where $\sigma\varepsilon$ is the turbulent Prandtl number and $C\varepsilon 1$, $C\varepsilon 2$, $C\varepsilon 3$ and $C\varepsilon 4$ are coefficients whose values are given bellow. The turbulent viscosity μt, is obtained via equation (16), with $f\mu$ set equal to unity.

$$\mu_t = f_\mu \frac{C_\mu \rho k^2}{\varepsilon} \tag{16}$$

$$S_{ij} = \frac{\partial u_i}{\partial x_j} + \frac{\partial u_j}{\partial x_i} \tag{17}$$

$C_{\varepsilon 1} = 1.44$, $C_{\varepsilon 2} = 1.92$, $C_{\varepsilon 3} = 0 < or > 1.44$,
$C_{\varepsilon 4} = -0.33$, $\sigma_k = 1.0$, $\sigma_\varepsilon = 1.22$

SIMPLE (Semi Implicit for Pressure-Linked Equations) algorithm can be explained as follow. If a steady-state problem is being solved iteratively, it is not necessary to fully resolve the linear pressure-velocity coupling, as the changes between consecutive solutions are no longer small. The main procedures for doing the SIMPLE algorithm are:

- An approximation of the velocity field is obtained by solving the momentum equation. The pressure gradient term is calculated using the pressure distribution from the previous iteration or an initial guess.
- The pressure equation is formulated and solved in order to obtain the new pressure distribution.
- Velocities are corrected and a new set of conservative fluxes is calculated

The computational code used was Star CD(Version 3.24), which solve the full 3D time dependent Navier-Stokes, continuity and energy equations using the finite volume method. It is widely used in the numerical simulation of different flow conditions in various complex geometries and was chosen in this study because it is proven capability and validity. The turbulent flow in this investigation is considered to be transient, incompressible, viscous, Newtonian and isotropic. The numerical solution involves splitting the geometry into many sub-volumes and then integrating the differential equations over these volumes to produce a set of coupled algebraic equations for the velocity components, and the pressure at the centre of each volume. The solver guesses the pressure filed and then solves the discretised form of the momentum equations to find new values of the pressure and velocity components. This process continues, in iterative manner, until the convergence criterion is satisfied. Turbulent model was using standard k-ε model. SIMPLE algorithm revised pressure and convection term belong to Upwind Scheme. Maximum residual tolerance was set under the 0.001 [5]. The geometry was drawn usin

g the CATIA (V5R15) CAD package and then imported to pro-Surf (Star CD's surface mesh generator) as an Initial Graphics Exchange Specification file (IGES). The computational mesh consists of 50,000 trimmed hexahedral cells. Inlet and outlet boundary conditions of snubber for CFD were applying the measured pressure from the experiment using pressure sensors at inlet (Point 1) and outlet (Point 6) for CFD. The model was built in a half type for the symmetrical shape of the snubber and the symmetry boundary condition was applied.

3. Result and discussion

3.1 Pressure characteristics analysis

The RMS values of gas pressures decrease with the distance from the compressor outlet along the snubber system. Data obtained from CFD analysis and the experiment show pressure characteristic of gas as in Fig. 3. Star-CD gives the pressure values at all points of the snubber system with the given inlet and outlet condition of pressure at point 1 and point 6. Point 1, 2 and 3 are in the inlet pipe at 7.5, 25.0, 45.0 cm; and point 4, 5 and 6 are in the outlet pipe of the snubber at 74.0, 94.0 and 111.5 cm, respectively, from compressor outlet. This shows that higher pressure at inlet side (point 2) and then the pressure is reduced and reached at outlet side (point 6) rejecting some pressure. The motor was set at 40hz, then data were taken at the different measuring points (point 1, 2, 3, 4, 5 & 6). CFD simulated data are 104.21192 KPa, 103.779 KPa, 102.1573 KPa and 101.85497 KPa, for point 2, point 3, point 4 and point 5, respectively. The experimental pressure values are 104.280981 KPa, 103.7094 KPa, 102.1275 KPa, 101.64819 KPa for those points. It shows that RMS values of CFD pressure are almost same with the experiment at each point in the snubber system. The highest pressure gradient is found between point 3 and point 4 for both CFD and Experment. Here the pressure drop is more than the other measuring points due to the main body of snubber. For 40Hz motor frequency, the input, output pressure and pressure loss are 103.773 KPa, 102.1527 KPa and 1.6217KPa for CFD; 103.7094 KPa, 102.1275 KPa and 1.5819 KPa for experiment, respectively. This indicates the best pressure restoring performance of the snubber.

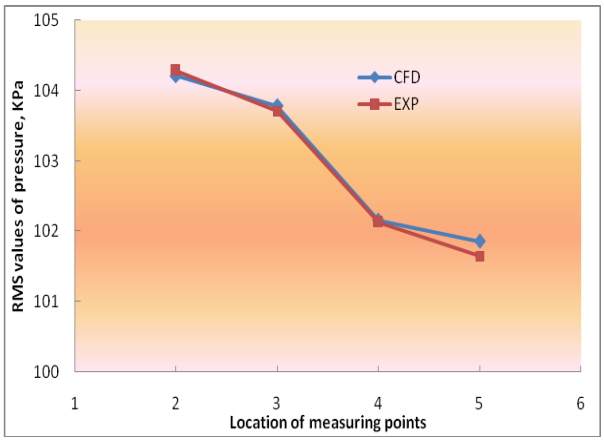

Fig. 3 RMS values of pressure against location of measuring points

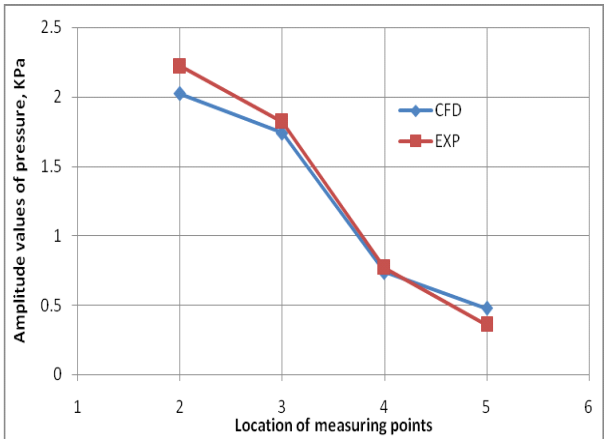

Fig. 4 Amplitude of pressure in the snubber system

The pressure amplitude values of the flowing gas through the snubber are shown for the both numerical and experiment (Fig. 4). It can be seen from this figure that the maximum pressure fluctuation is occurred at point 1 and then it follows by point 2, point 3, point 4 and

point 5. The amplitude of pressure drop abruptly drops down between point 3 and point 4 due to the buffering action of the main tube shape. Tube shaped buffered snubber reduces its incoming amplitude 1.738957 KPa to 0.737153 KPa, a considerable amount for CFD. The experiment also gives almost same value as CFD. Detail pictures are as in Fig. 4. The amplitude reduction by the snubber is 1.001804 KPa for CFD and 1.0509596 KPa for experiment.

3.2 CFD simulation of pressure in the snubber

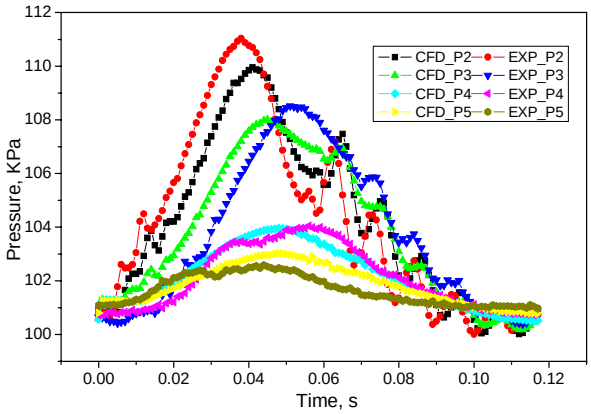

Fig. 5 CFD simulated and experimental pressure at snubber system

CFD can be applied to study pressure characteristics through the snubber. The solution of continuity equation, Navier Stoke's momentum equation and energy equation by STAR-CD 3.24 give the pressure in the snubber system. Experimental pressure value at point 2, point 3, point 4 and at 5 with the CFD simulated corresponding values against time are presented in Fig. 5 for 40 Hz. CFD simulated pressures are almost same behaviors those of pressure values find experimentally at these points. Mongst them point 2 and point 3 shows more irregular in shape and several dominant peaks whereas in point 4 and point 5 pressure values have down blunt peaks for both CFD and experiment which is the outcome of snubber main body. All these As CFD calculated pressures at point 2, 3, 4, and 5 are well match with the experiment, so, it can allow the CFD simulation of pressure distribution inside the snubber system.

The description of the pressure in the inlet pipe, inside the snubber including at buffer, and outlet pipe can be found at every time step. Fig. 6 explains the pressure values in the snubber system with pictorial, numerical, maximum and minimum values. High pressure is developed at the beginning in the inlet pipe (Fig. 6(a), 6(b)) and it dwindles gradually with length of pipe. But there is sudden pressure drop from point 3 to point 4 due to snubber main body. Inside the snubber main unit, the entrance point of snubber (Fig. 6(c)), below the buffer parallel to inlet pipe (Fig. 6(d)), exit pipe entrance (6(e)) has high pressure zones. The pressures become weaken largely and reaches 0.8519E+05 Pa at outlet of the system (Fig. 6(f). At the beginning of time step, there form different pressures at various points but at end of time step it is demolished and then pressure is become well distributed throughout the snubber but some locations. At the time step of t=0.31E-01 s, the maximum and minimum pressure are 0.1108E+06 Pa and 0.8519E+05 Pa, respectively at the entrance and exit point in the snubber system. Detail pressure distribution with graphical and numerical values at various time steps can be obtained by selecting specific zone of the snubber model in CFD.

4. Conclusion

Instantaneous measurement of pressure at various points in the snubber system can give the pulsation and its reduction information. It is possible only by computer aided CFD program. Numerical solution of various equations using CFD is a now-a-days tool to calculate pressure distribution in a system. In

this study, CFD predicts pressure pulsation reduction as 1.001804 KPa and by experiment 1.0509596 KPa pressure pulsation reductions is found. The percentage of pressure losses are estimated at 1.6217 KPa and 1.5819 KPa, for CFD simulation and by experiment, respectively. So, CFD can be used for detail distribution of pressure pulsation and pressure loss at the snubber in hydrogen compression system.

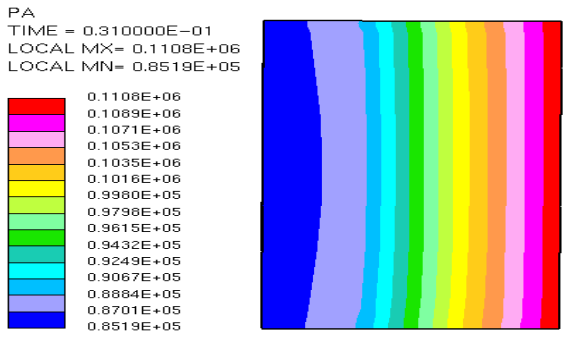

(a) Pressure distribution legend (b) Inlet pressure at snubber system

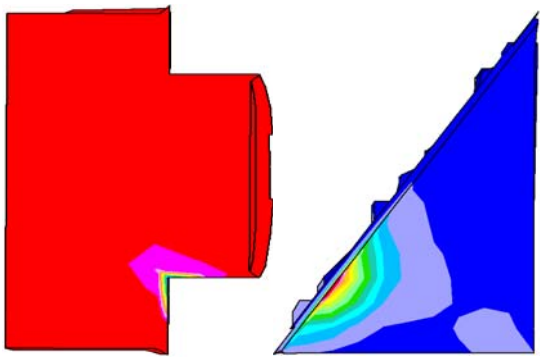

(c) Inlet of main tube (d) At the buffer surface

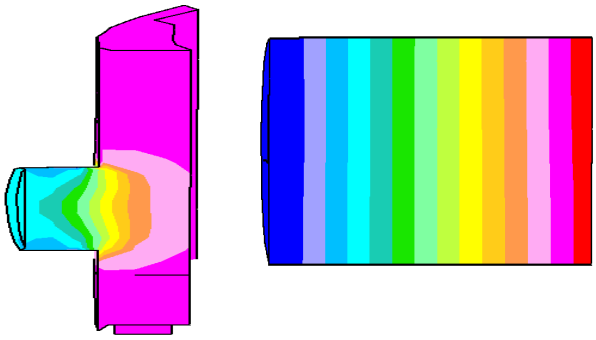

(e) Exit of tube (f) At the exit point 6

Fig. 6 Pressure distribution inside the snubber system

Acknowledgment

This research was supported under the project No. 10024337 and Program for the Training of Graduate Students in Regional Innovation System of the Ministry of Knowledge Economy and Second-Phase of BK 21 project, Korea.

Reference

1. Midili, A. and Dincer, I., Key strategies of hydrogen energy systems for sustainability, Int J. of Hydrogen Energy 32, 511-524 (2007).
2. Forsberg, P. and Karlstrom, M., On optimal investment strategies for a hydrogen refueling station, Int J. of Hydrogen Energy 32, 647-660 (2007).
3. Ogden, J.M., Developing an infrastructure for hydrogen vehicles: a Southern California case study, Int J. of Hydrogen Energy 24, 709-730 (1999).
4. Origin lab Co. 2003. Origin Reference v7.5. FFT Mathematical Description.
5. Star CD Methodology.